REAL-TIME MONITORING OF LOCALIZED AND GENERAL CORROSION RATES IN DRINKING WATER SYSTEMS UTILIZING COUPLED MULTIELECTRODE ARRAY SENSORS

Xiaodong Sun and Lietai Yang
Corr Instruments, LLC
San Antonio, TX, USA

ABSTRACT

Real-time monitoring for localized and general corrosion rates of carbon steel, brass, and stainless steel materials was conducted in low-conductivity waters utilizing coupled multielectrode sensors at ambient temperature. It was demonstrated that the coupled multielectrode sensors are effective real-time tools for monitoring the localized and general corrosion rates in air-saturated waters. The steady-state maximum localized corrosion rates measured in the air-saturated natural spring water were found to be approximately 1 µm/yr (0.04 mil/yr) and 0.03 µm/yr (0.0012 mil/yr) for Type 260 brass and Type 316L stainless steel, respectively. The steady-state maximum pitting corrosion rate for the Type 1008 carbon steel was found to be approximately 1 mm/yr (40 mil/yr). Localized corrosion penetration depth factors, which are defined as the ratios of the cumulative maximum localized penetration depth to the cumulative general corrosion depth, were found to be approximately 11 for the brass, 4 for the carbon steel, and 2 for the stainless steel after two hours of immersion in the natural spring water. It was also demonstrated that the coupled multielectrode sensors were proficient tools for the measurement of the effectiveness of cathodic protection in the water system.

Keywords: Corrosion monitoring, corrosion in water, pitting rate, corrosion sensor, localized corrosion, online corrosion sensor, corrosion probe, real-time corrosion sensor, multielectrode sensor, coupled multiple electrodes, cathodic protection, corrosion rate.

INTRODUCTION

Corrosion of metallic components in drinking water systems has been an ongoing concern. According to a recent report,[1] the total estimated cost of corrosion for drinking water systems is $19.26 billion per year, in the United States alone. To effectively control and mitigate corrosion, it is important to measure the real-time rate of corrosion—especially the rate of localized corrosion—taking place in the system. Coupled multielectrode sensors (CMAS) have been recently used as *in situ* and online monitors for localized corrosion, in the cooling water pipes of chemical plants[2-3] and other laboratory

and field systems. [4-19] Some of the CMAS applications include quantitative and real-time localized corrosion monitoring for cathodically protected systems,[10] coated metal components,[11,16] metals in concrete,[12] metals in soil,[15] and in simulated marine environments.[18] The coupled multielectrode probes were also used as a real-time corrosion monitor for the propagation rate of crevice corrosion for stainless steel and carbon steel in simulated seawater.[19] In the present work, coupled multielectrode corrosion probes were used as an online tool for measuring the general and maximum localized corrosion rates of metals in drinking water systems. These metals include low carbon steel, stainless steel and brass. The experimental results of the general and localized corrosion rates obtained in different waters, with and without cathodic protection, are presented in this paper.

EXPERIMENTAL PROCEDURES

A nanoCorr[TM*]S-50 coupled multielectrode analyzer,[20] manufactured by Corr Instruments (San Antonio, TX, USA), was used in the experiment (*Figure 1*). The coupled multielectrode corrosion analyzer shown in *Figure 1* allows the measurement of coupling currents for up to 50 electrodes. With the factory supplied CorrVisual[TM*] software, this analyzer simultaneously measures the real-time localized corrosion rates and penetration depth, average/general corrosion rates and penetration depth, corrosion potentials, temperature and other parameters from: four independent coupled multielectrode probes, three pH or three oxidation/reduction potential (ORP) probes, or three other transducers for parameters, such as conductivity, humidity, flow, and pressure. In this experiment, the analyzer was used with three 16-electrode multielectrode probes, one temperature probe, one pH probe, and one ORP probe made of platinum.

Figure 2 shows typical coupled multielectrode probes for general and localized corrosion rate monitoring. *Figure 3* shows the principle of the coupled multielectrode corrosion analyzer.[12,15] The analyzer couples the multiple sensing electrodes, made of the same material as that used in a given application, to a common joint through resistors. In a non-uniform corrosion condition (e.g., localized corrosion conditions), some of the electrodes corrode in preference to others and, therefore, a dispersion in the measured currents from the sensing electrodes is observed. Thus, the multiple electrodes in the probe simulate a single piece of metal.[5-6] If the sensing elements are sufficiently small, so that separation of anodic and cathodic reactions between different electrodes can be assumed, the localized corrosion rates can be obtained directly from the measured current densities, which correspond to non-uniform corrosion.

The experiment was conducted in a beaker filled with distilled water or natural spring water. The natural spring water was supplied by Ozarka Spring Water Company (Greenwich, Connecticut, USA). All coupled multielectrode probes (one carbon steel, one stainless steel and one brass); one temperature probe, one pH probe, and one oxidation and reduction potential (ORP) probe were vertically immersed in the water. Prior to the tests, the distilled water and the spring water were placed in the open air to enable saturation with the gases in the atmosphere (e.g. O_2 and CO_2). The waters were not agitated during the experiments. Three aluminum wires (1 mm diameter) were used as sacrificial anodes to simulate the cathodic protection condition. The immersion depth of the wire in the water was approximately 5 cm. The ORP probe has a built in saturated Ag/AgCl reference electrode. A saturated calomel electrode (SCE) was used as the reference electrode for measurements of the electrochemical potentials of the probes. The experiments were conducted at a temperature range from 17 to 23 ^{o}C.

The sensing electrodes of the carbon steel multielectrode probe were made from annealed Type 1008 carbon steel (UNS G10080) wire (1.5 mm in diameter and 1.77 mm^2 in electrode surface area). The sensing electrodes of the brass multielectrode probe were made from Type 260 brass (UNS C26000) wire (1 mm in diameter and 0.785 mm^2 in electrode surface area). The sensing electrodes of the stainless steel multielectrode probe were made from Type 316L (UNS S31603) wire (1 mm in diameter and 0.785 mm^2 in electrode surface area). Each probe had 16 electrodes flush-mounted in epoxy. Prior to the test, the surfaces of the sensing electrodes for each multielectrode probe were polished to 600 grit and rinsed with distilled water and then with acetone.

A notebook computer was used to collect the data from the multielectrode analyzer. The current from each electrode, the electrochemical potential (the coupling potential) of each probe, and the temperature were logged at a predetermined interval (usually 20 to 600 seconds) and saved in a computer file. Processed signals (such as the maximum localized corrosion current, the cumulative charge for each sensor, average corrosion rate, maximum localized corrosion rate, cumulative maximum localized corrosion penetration depth, and cumulative average corrosion penetration depth for each probe) were also saved in one or more separate data files. During the measurements, all the directly measured currents and the processed results (such as the minimum current, maximum current, mean current, current densities, corrosion rates, cumulative charges, penetration depth, and electrochemical potential) were dynamically displayed from the computer screen, in both numerical and graphical forms. The configuration parameters for data acquisition were also available on the computer screen.

Figure 4 shows a schematic diagram for the wiring configuration between the multielectrode probes, the reference electrode, and the sacrificial anodes with the multielectrode corrosion analyzer, during the cathodic protection test.

RESULTS AND DISCUSSIONS

Short-Term Testing and Cathodic Protection

Figure 5 shows the measured maximum localized corrosion rates and the potentials of the Type 316L stainless steel, Type 260 brass, and low carbon steel probes, and the temperature, pH and ORP of the water during a short-term testing in distilled water and natural spring water, with and without cathodic protection. Detailed results for maximum localized corrosion rates, average or general corrosion rates, electrochemical potentials and temperature, pH and oxidation/reduction potential (ORP), are presented and discussed as follows:

Maximum Localized Corrosion Rates. The maximum localized corrosion rates from the software are presented in *Figure 6*. The maximum localized corrosion rate from a probe is calculated using the anodic current density from the most corroding electrode of the probe.[18] The maximum localized corrosion rates were 0.17, 7.0, and 90 µm/yr (0.0067, 0.28, 3.5 mil/yr), for the 316L stainless steel, 260 brass, and low carbon steel probes, respectively. On moving the probes from the beaker containing distilled water to a beaker containing natural spring water, the maximum localized corrosion rate of the carbon steel probe increased to 330 µm/yr (13 mil/yr) in two hours. There were, however, no significant changes in the maximum localized corrosion rates from the Type 260 brass and the Type 316L stainless steel probes after the change of water. When the electrodes of the three probes were connected to their respective sacrificial aluminum anodes, the maximum localized corrosion rates of the Type 316L stainless steel and the Type 260 brass immediately dropped below the detection limit of the instruments (10 nm/yr or 0.0004 mil/yr), suggesting that these two probes were sufficiently cathodically protected by the potential (see the Probe Potential section below) supplied by their sacrificial anodes.

The maximum localized corrosion rate of the carbon steel probe, however, only decreased slightly (from 330 to 290 µm/yr), when the probe was connected to the aluminum anode, indicating an insufficient cathodic protection. The insufficient protection by the aluminum anode is consistent with the relatively high potential (see the Probe Potential section below) supplied by the sacrificial anode, because of its limited surface area.

Average and General Corrosion Rates, and Localized Corrosion Rate Factors. The average corrosion rates from the software are presented in *Figure 7*. The average corrosion rate from a probe is calculated using the average anodic current, which is the total anodic currents from all the electrodes of the probe divided by the total surface areas of all the electrodes of the probe.[18] Because this average corrosion rate is similar to the general corrosion rate obtained by weight loss methods or by other electrochemical methods using large electrodes, the average corrosion rate may be used to estimate the general corrosion rate. Compared with *Figure 6*, the average/general corrosion rates from these three metals have similar trends with the maximum localized corrosion rates, but the values are much smaller. The ratio of the maximum localized corrosion rate to the average corrosion rate is called localized corrosion rate factor.[18] The real-time localized corrosion rate factors for the three metals are presented in *Figure 8*. The maximum localized corrosion rates were 7.5 to 8 times higher than their average corrosion rates for the Type 260 brass and low carbon steel during the test. The ratio of the maximum localized corrosion rate to the average corrosion rate for the Type 316 stainless steel was approximately 4 in the distilled water and it increased to approximately 9, at the end of the spring water test.

Maximum Localized Corrosion and Average Corrosion Depths, and Localized Corrosion Depth Factors. The real-time maximum localized corrosion penetration depths and average corrosion depths calculated by the software for the three metals are presented in *Figures 9* and *10*, respectively. The maximum localized corrosion depth, at a given time, is the depth on the most corroded electrode (or deepest pit, if the localized corrosion is in the form of pitting corrosion) of the probe at the time.[18] The average depth is the sum of the total depth on all electrodes divided by the total surface areas of all electrodes of the probe. The average corrosion depth is equivalent to the general corrosion depth obtained by the weight loss method or by other electrochemical methods using large electrodes. The ratio of the maximum localized corrosion penetration depth (values shown in *Figure 9*) to the average corrosion depth (values shown in *Figure 10*) is defined as the localized corrosion depth factor.[18] The real-time localized corrosion depth factors for the three metals are presented in *Figure 11*. The localized corrosion depth factor for the Type 260 brass was higher than 8 throughout the test, and 11 at the end of the two hours in spring water, indicating that the corrosion on the brass was highly non-uniform (or localized), even though the maximum localized rate was low (<10 µm/yr or <0.4 mil/yr, see *Figure 6*). The localized corrosion depth factor for the Type 316L stainless steel was less than 3 throughout the testing period, and 2 at the end of the two hours in spring water, indicating that the extremely low corrosion rate on the stainless steel (maximum localized rate <0.2 µm/yr or 0.008 mil/yr, see *Figure 6*) was relatively uniform and there was no significant localized corrosion. The localized corrosion depth factor for the low carbon steel probe was high (>8) in the distilled water and decreased to approximately 4 at the end of the test in the spring water, indicating that as corrosion continued, the corrosion on the carbon steel tended to be less non-uniform in the spring water.

Probe Potentials and Water Temperature. The corrosion potentials of the Type 316L stainless steel, Type 260 brass, and Type 1008 carbon steel probes in the distilled water were -20, -100, and -360 mV (SCE), respectively (*Figure 12*). The corrosion potentials of the 316L stainless steel, and the 260 brass probes in the spring water remained essentially the same as in the distilled water. The corrosion potential of the carbon steel probe increased slightly (by 40 mV), immediately after the change from distilled water to spring water. During the two hours in spring water, the carbon steel corrosion potential

decreased steadily from -318 mV (SCE) to -374 mV(SCE), indicating that the carbon steel electrode became more and more active, which is consistent with the measured steadily increased maximum localized corrosion rate from the carbon steel probe as shown in *Figure 6*. When the electrodes of the three probes were connected to their sacrificial aluminum anodes, the potentials of the Type 316L stainless steel and the Type 260 brass probes immediately dropped by more than 400 mV and 100 mV, respectively; the potential of the carbon steel electrode, however, dropped only by 10 mV. The variations in the drops of the potentials, during the cathodic protection, were due to the size of the aluminum anodes used as the sacrificial anodes. The surface areas of the aluminum anodes were sufficiently large enough to lower the potentials of the less active stainless steel and brass probes, but not enough to lower the potential of the more active carbon steel probe. Because of the significant drop in potentials, the stainless steel and brass probes were effectively protected and their corrosion rates were essentially zero (see *Figure 6*), while the slight drop in potential for the carbon steel probe proved to be insufficient for the carbon steel to be cathodically protected and its maximum localized corrosion rate remained essentially unchanged (from 330 to 290 µm/yr) (*Figure 6*).

The temperature of the distilled water was approximately 17 $^\circ$C and the temperature of the spring water was approximately 18 $^\circ$C.

Oxidation/Reduction Potential and pH of the Waters. The oxidation/reduction potential (ORP) was at approximately 315 mV (Ag/AgCl), during the test with distilled water (*Figure 13*). The potential suddenly increased, from approximately 315 to 328 mV (Ag/AgCl), when the probe was moved from the distilled water into the spring water. The sudden change may be due to the change in pH (from 5.99 to 5.88, see next paragraph) and the slightly higher temperature of the spring water than that of the distilled water, because the ORP was essentially controlled by the oxygen reduction reaction on the platinum electrode, which involves a hydrogen ion, and has a better kinetics at a higher temperature. The ORP gradually increased by 40 mV (from 328 to 367 mV [Ag/AgCl]), during the two-hour immersion in the spring water. The cause for such gradual increase in ORP is not known, but it is, however, not unusual to see such small fluctuations in ORP in water, even though the chemistry of the water appeared to be the same.[2] The ORP abruptly dropped from 357 to 316 mV (Ag/AgCl) at the time the three multielectrode probes were connected to their sacrificial anodes for cathodic protection. This drop was probably caused by the change in the spatial potential distribution caused by the flow of the cathodic protection currents in the water.

The pH of the distilled water was approximately 6.0, with a slight decrease from 6.02 at the beginning, to 5.99 at the end (*Figure 13*). The pH of the spring water was 5.88 initially, but fluctuated slightly between 5.88 and 5.98, during the two-hour immersion test. The slight acidity in the two waters was probably due to the absorption of CO_2 from the atmosphere.

Longer-Term Testing in Natural Spring Water

Figure 14 shows the measured maximum localized corrosion rates and the potentials of the Type 316L stainless steel, Type 260 brass, and Type1008 carbon steel probes, and the temperature, pH, and ORP of the water, during an eight-day testing in the air-saturated spring water. Separate plots are given for the maximum localized corrosion rates, electrochemical potentials and temperature, and pH and ORP in *Figures 15, 16*, and *17*, respectively. The maximum localized corrosion rates were initially high for the brass (7.2 µm/yr or 0.28 mil/yr) and stainless steel (0.30 µm/yr or 0.012 mil/yr), but gradually decreased, in 4.5 days, to approximately 1 µm/yr (0.04 mil/yr) and 0.03 µm/yr (0.0012 mil/yr), respectively (see *Figure 15*). The localized corrosion rate for the brass and stainless steel did not change in the remaining 3.5 days of testing. The maximum localized corrosion rate for the Type 1008 carbon

steel was initially low (88 µm/yr or 3.5 mil/yr), but increased to 1 mm/yr (40 mil/yr) in less than two days. Then, the maximum localized corrosion rate of the carbon steel probe remained at 1 mm/yr (40 mil/yr), in the remaining 6 days of testing.

The stabilized maximum localized corrosion rates for the three metals varied by nearly 5 orders of magnitude, from 30 nm/yr (0.0012 mil/yr), for the type 316L stainless steel, to 1 mm/yr (40 mil/yr), for the Type 1008 carbon steel (*Figure 15*). The 316L stainless steel material was essentially not corroding in the air-saturated natural spring water. Because all the probes were polished to 600 grit prior to the start of the test, the relatively initial high maximum localized corrosion rates for the brass and stainless steel probes were probably due to the fresh surface on the electrodes. After 2.5 days of immersion, the electrodes were probably covered by a thin layer of oxides and were passivated. As a result, no significant sustainable localized corrosion was taking place. The behavior of the localized corrosion of carbon steel probe is the opposite to those of the other two metals. It was low when the surface was initially fresh and increased, as the corrosion on the electrode surface progressed, indicating that the metastable localized corrosion requires the formation and stabilization of sustainable anodic sites.

The corrosion potentials of the 316L stainless steel and 260 brass in the natural spring water were between 0 and -100 mV (SCE) (*Figure 16*) and did not change significantly over the course of the test. This range of potential is relatively noble and so it is consistent with the low maximum localized corrosion rates for these two metals, as shown in *Figure 15*. The corrosion potential of the carbon steel probe was relatively high (-320 mV [SCE]) initially, and decreased to and stabilized at approximately -580 mV [SCE], after the first 2.5 days of immersion. The initial relatively noble potential of the carbon steel probe is consistent with the initial low maximum localized corrosion rate, and the relatively active potential observed 2.5 days after the start of the test is consistent with the high maximum localized corrosion rate (see *Figure 15*).

The ORP of the natural spring water was approximately 350 mV (Ag/AgCl) at the beginning of the test and decreased rapidly in the first two days and then slowly during the remaining six days, reaching approximately 100 mV (Ag/AgCl) at the end of the test (*Figure 17*). The pH of the spring water was approximately 5.9 at the beginning of the test and increased rapidly in the first two days and then slowly during the remaining six days, reaching approximately 6.6 at the end (*Figure 17*). Part of the decrease in the ORP value was likely due to the increase in pH. It is not known, however, what caused the increase in pH and what other causes for the decrease in the ORP are, because the small pH change could not account for the ORP drop, as large as 200 mV.

Post Test Visual Examination

Figure 18 shows the appearance of the 260 brass and 316L stainless steel probe electrodes after the eight-day testing in the natural spring water. No localized corrosion was seen in the two probes, even though a slight discoloration was observed on some of the electrodes of the Type 260 brass probe, which is consistent with the low maximum localized corrosion rates, as shown in *Figure 15*. *Figure 19* shows the appearance of the carbon steel probe after the eight-day testing. It is apparent that a few of the electrodes were covered by deposits (corrosion products), and most of others were clean. After cleaning off the corrosion products, pitting was observed on the electrodes covered by the deposits. No pitting corrosion was observed on the electrodes that did not have deposits. Therefore, the deposit-covered electrode served as the anodes and the clean electrodes served as the cathode, during the testing. The pitting corrosion on the carbon steel probe is consistent with the high maximum localized corrosion rate

as shown in *Figure 15*. It is worth mentioning that no significant corrosion between the electrodes and the surrounding epoxy was observed.

CONCLUSION

Real-time coupled multielectrode array sensor probes were used to measure the maximum localized corrosion rates of Type 316L stainless steel, Type 260 brass, and Type 1008 carbon steel materials in low-conductivity waters. The maximum localized corrosion rates in both the distilled water and the natural spring water were the same for the stainless steel (0.03 to 0.3 µm/yr [0.0012 to 0.012 mil/yr]) and brass (1 to 7.2 µm/yr [0.04 to 0.28 mil/yr] at ambient temperatures (17 to 23 ^{o}C). The steady-state maximum localized corrosion rate for the carbon steel in natural spring water was found to be 1 mm/yr (40 mil/yr). Visual examination on the electrodes of the carbon steel probe showed that the localized corrosion was in the form of pitting corrosion, rather than crevice corrosion. The ratios of the cumulative maximum localized corrosion penetration depth to the cumulative general corrosion depth were found to be approximately 11 for the brass, 4 for the carbon steel and 2 for the stainless steel, after two hours of immersion in the natural spring water. The pH of the air-saturated distilled water and air-saturated natural spring water was slightly acidic (5.8 to 6.3). It was also shown that the coupled multielectrode array sensor probes were useful tools for measuring the effectiveness of cathodic protection. The maximum localized corrosion rates for the brass and stainless steel probes decreased to essentially zero when the probes were cathodically polarized at sufficiently low voltages; the maximum localized corrosion rate for the carbon steel probe decreased only slightly when the surface area of the sacrificial anode was too small to cathodically polarize the carbon steel electrodes.

REFERENCES

1. G. H. Koch, M.P.H. Brongers, N.H. Thompson, Y. P. Virmani, and J.H. Payer, "Corrosion Cost and Preventive Strategies in the United States," NACE Report, FHWA-RD-01-156, (Houston, TX: NACE, 2001).

2. M. H. Dorsey, L. Yang and N. Sridhar, "Cooling Water Monitoring Using Coupled Multielectrode Array Sensors and Other On-line Tools," CORROSION/2004, paper no. 04077, (Houston, TX: NACE International, 2004).

3. Michael H. Dorsey, Daniel R. Demarco, Brian J. Saldanha, George A. Fisher, Lietai Yang and Narasi Sridhar, "Laboratory Evaluation of a Multi-Array Sensor for Detection of Underdeposit Corrosion and/or Microbially Influenced Corrosion," CORROSION/2005, paper no. 05371 (Houston, TX: NACE, 2005).

4. L. Yang and N. Sridhar, "Monitoring of Localized Corrosion ASM Handbook," Volume 13A-Corroson: Fundamentals, Testing, and Protection, Stephen. D. Crammer and Bernard S. Covino, Jr. Eds, ASM International, Materials Park, Ohio, 2003, pp 519-524.

5. L. Yang, N. Sridhar, O. Pensado, and D.S. Dunn, *Corrosion*, 58 (2002), p.1004.

6. L. Yang and N. Sridhar, "Coupled Multielectrode Online Corrosion Sensor," Materials Performance, 42 (9), pp 48-52 (2003).

7.   L. Yang, R.T. Pabalan, L. Browning, and G.C. Cragnolino, "Measurement of Corrosion in Saturated Solutions under Salt Deposits Using Coupled Multielectrode Array Sensors," CORROSION/2003, paper no. 426 (Houston, TX: NACE, 2003).

8.   L. Yang, R. T. Pabalan, L. Browning and D.S. Dunn, "Corrosion Behavior of Carbon Steel and Stainless Steel Materials under Salt Deposits in Simulated Dry Repository Environments," in Scientific Basis for Nuclear Waste Management XXVI R. J. Finch and D. B. Bullen eds, Warrendale, PA: Materials Research Society, M.R.S. Symposium Proceedings Vol. 757, pp.791-797, 2003.

9.   C.S. Brossia and L. Yang, "Studies of Microbiologically Induced Corrosion Using a Coupled Multielectrode Array Sensor," CORROSION/2003, paper no. 575 (Houston, TX: NACE, 2003).

10. X. Sun, Xiaodong Sun, "Online Monitoring of Corrosion under Cathodic Protection Conditions Utilizing Coupled Multielectrode Sensors," CORROSION/2004, paper no. 04094, (Houston, TX: NACE International, 2004).

11. X. Sun, "Online Monitoring of Undercoating Corrosions Utilizing Coupled Multielectrode Sensors," CORROSION/2004, paper no.04033 (Houston, TX: NACE, 2004).

12. X. Sun, "Online and Real-Time Monitoring of Carbon Steel Corrosion in Concrete, Using Coupled Multielectrode Sensors," CORROSION/2005, paper no.05267 (Houston, TX: NACE, 2005).

13. Lietai Yang, Darrell Dun and Gustavo Cragnolino, "An Improved Method for Real-time and Online Corrosion Monitoring Using Coupled Multielectrode Array Sensors," CORROSION/2005, paper no. 05379 (Houston, TX: NACE International, 2005).

14. Lietai Yang, Darrell Dun, Yi-Ming Pan and Narasi Sridhar, "Real-time Monitoring of Carbon Steel Corrosion in Crude Oil and Salt Water Mixtures Using Coupled Multielectrode Sensors," CORROSION/2005, paper no. 05293, (Houston, TX: NACE International, 2005).

15. Xiaodong Sun, "Real-Time Corrosion Monitoring in Soil with Coupled Multielectrode Sensors," CORROSION/2005, paper no.05381 (Houston, TX: NACE, 2005).

16. Xiaodong Sun, "Online Monitoring of Undercoating Corrosion Using Coupled Multielectrode Sensors," Materials Performance, 44 (2), p28-32 (2005).

17. A. Anderko, N. Sridhar1 and L. Yang, S.L. Grise, B.J. Saldanha, and M.H. Dorsey, "Validation of a Localized Corrosion Model Using Real-Time Corrosion Monitoring in a Chemical Plant," Corrosion Engineering, Science and Technology (formerly British corrosion J.), Vol. 40, pp.33-42, August, 2005

18. Xiaodong Sun and Lietai Yang, "Real-Time Monitoring of Localized and General Corrosion Rates in Simulated Marine Environments Using Coupled Multielectrode Array Sensors," CORROSION/2006, paper no.06284 (Houston, TX: NACE, 2006).

19.   Xiaodong Sun, "Real-Time Monitoring of Crevice Corrosion Propagation Rates in Simulated Seawater Using Coupled Multielectrode Array Sensors," CORROSION/2006, paper no.06679 (Houston, TX: NACE, 2006).

20.   Corr Instruments, "nanoCorr S-50 Multielectrode Analyzer for Real-Time Monitoring of Corrosion Rate, pH, ORP and Others," Materials Performance, 44 (3), p100 (2005).
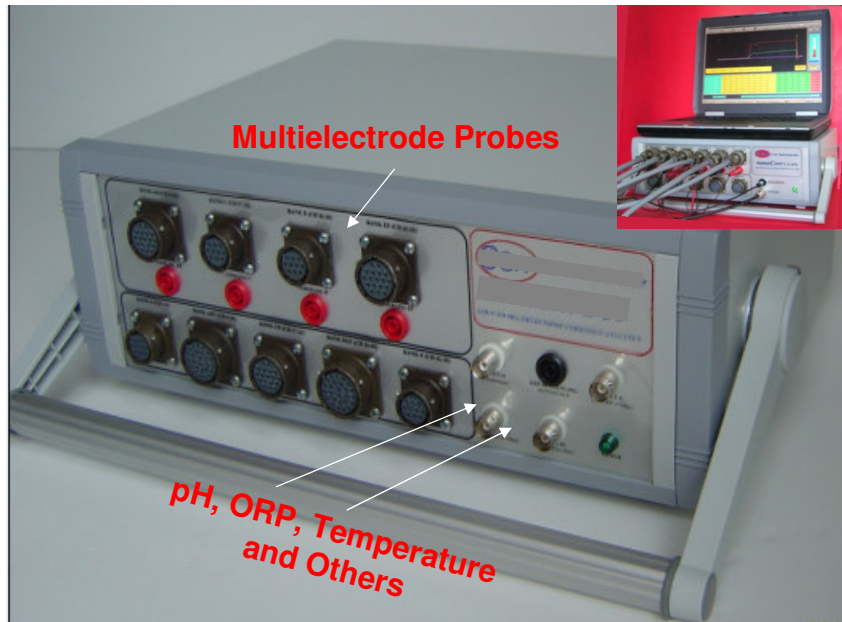
Figure 1. Coupled multielectrode analyzer used in the experiments and typical real-time displays on a notebook computer (see insert).

Note: This analyzer simultaneously measures the real-time localized corrosion rates and penetration depths, average corrosion rates and penetration depths, corrosion potentials, temperature, and other parameters from: 4 independent coupled multielectrode probes, 3 pH or 3 ORP probes, or 3 other transducers for parameters such as conductivity, humidity, flow, and pressure.

Figure 2. Typical coupled multielectrode array sensor probes.
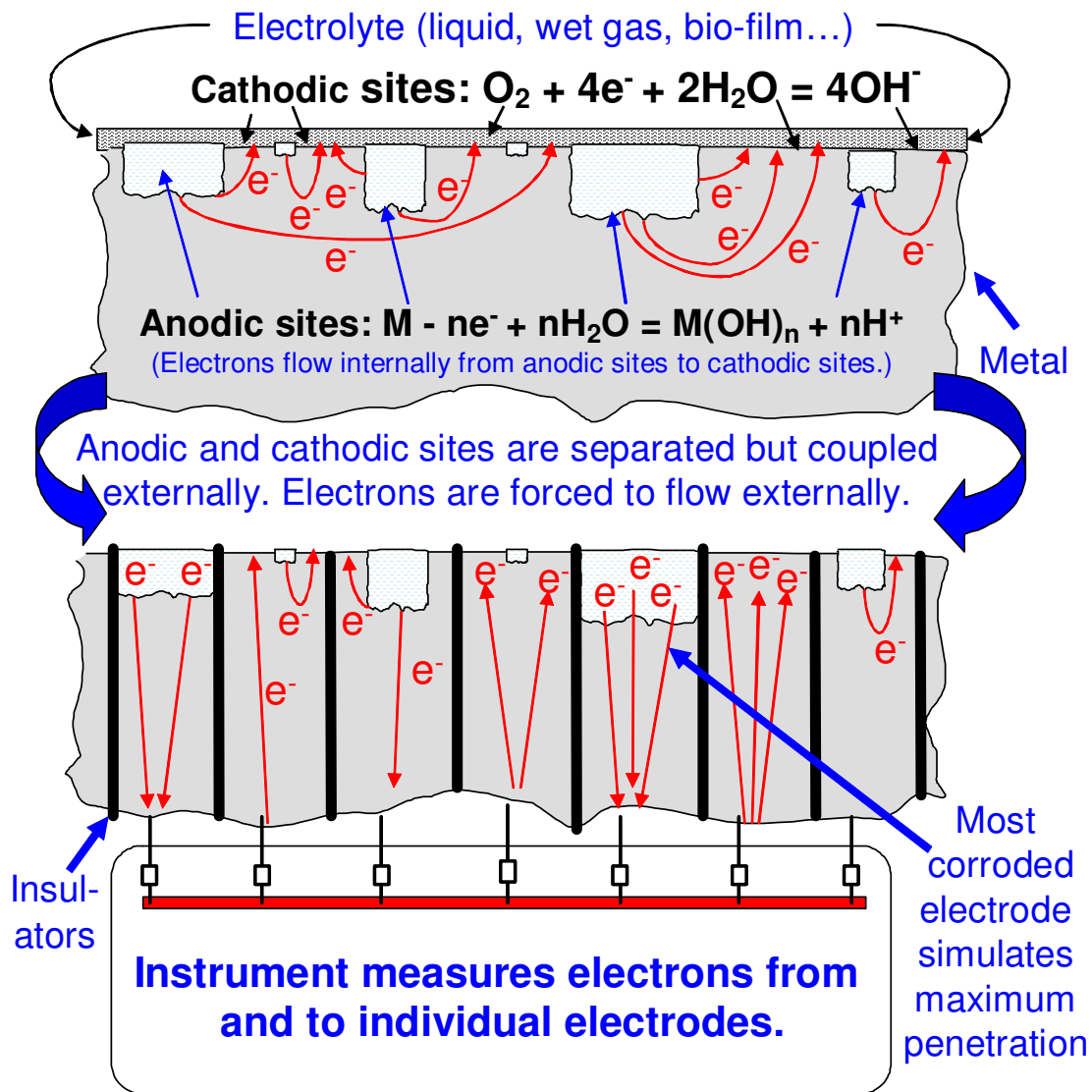
Figure 3. Schematic diagram showing the principle of the coupled multielectrode array sensor analyzer for the measurement of localized corrosion.[12-13,15] **The maximum localized corrosion rate from the instrument represents the penetration rate of the most corroding electrode (e.g., 3rd from the right in the bottom figure). The maximum localized penetration depth from the instrument represents the corroded depth of the most corroded electrode.**[12] **The general or average corrosion rate is calculated from the average of the anodic currents, and the general or average corrosion depth is calculated from the average of the anodic charges.**[18]
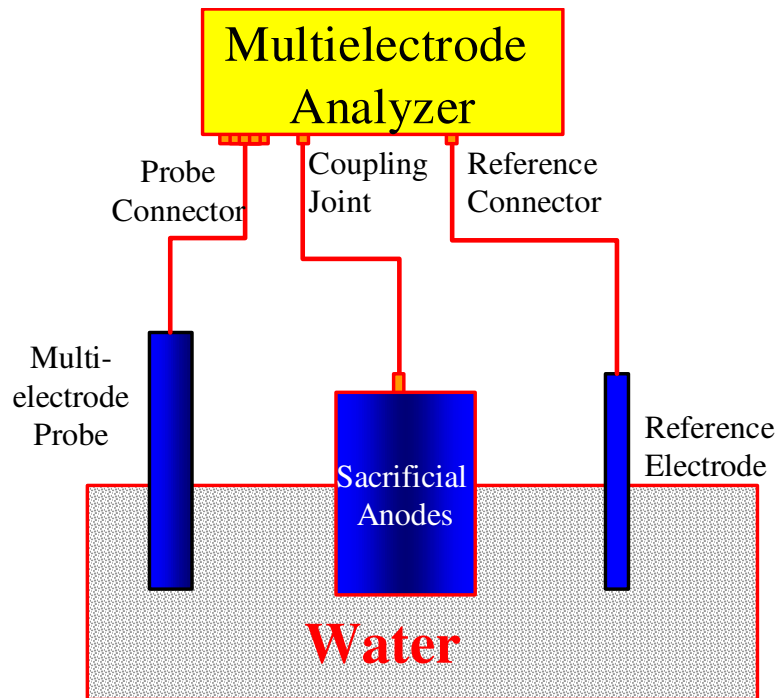
**Figure 4. Schematic diagram showing the wiring configuration during the cathodic protection test.**
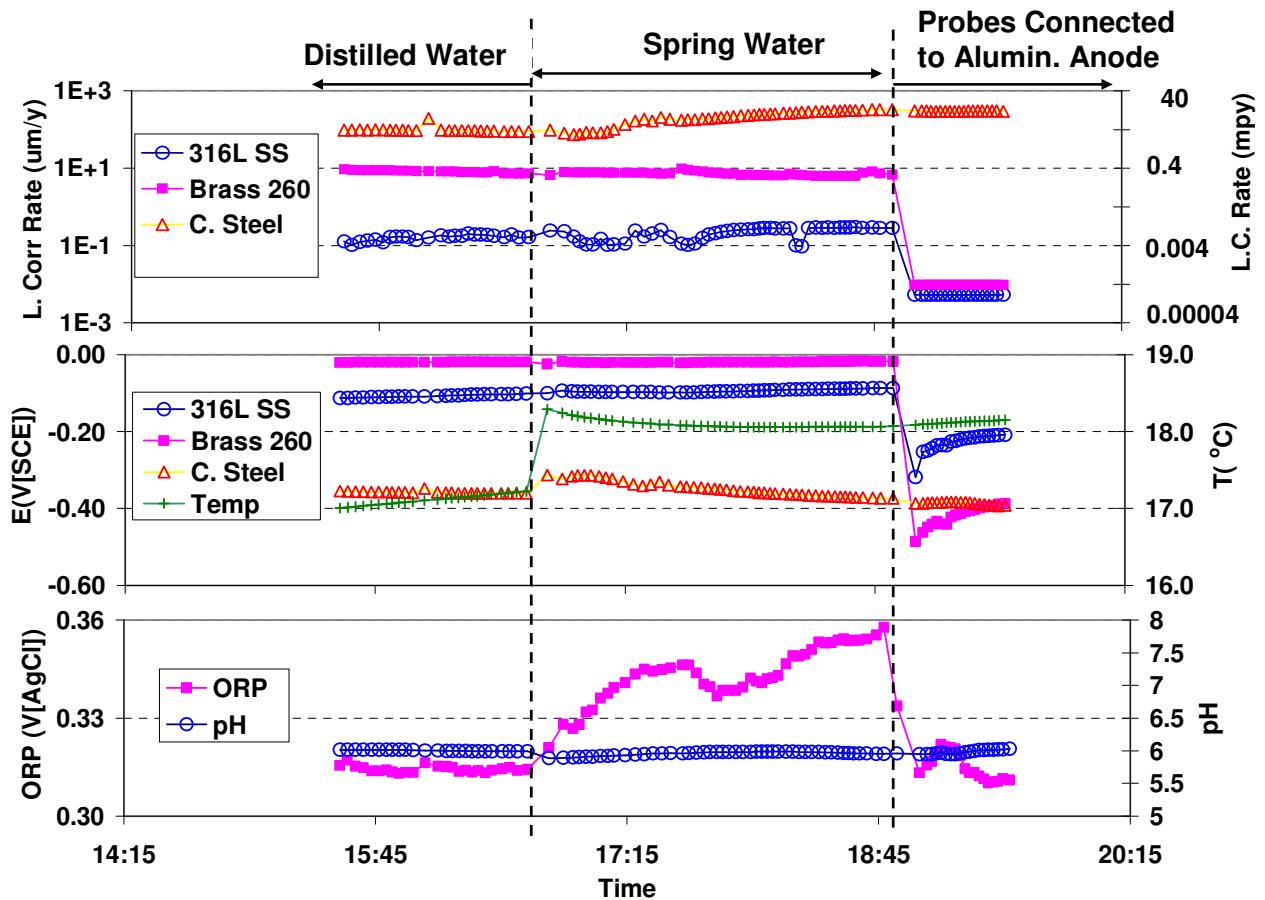
Figure 5. Maximum localized corrosion rates and the potentials of Type 316L stainless steel, Type 260 brass, and Type 1008 carbon steel probes; temperature, pH, and ORP of the water, during a short-term testing with and without cathodic protection.
Note: Probe electrodes were connected to aluminum anodes to simulate cathodic protection condition (See Figure 4).
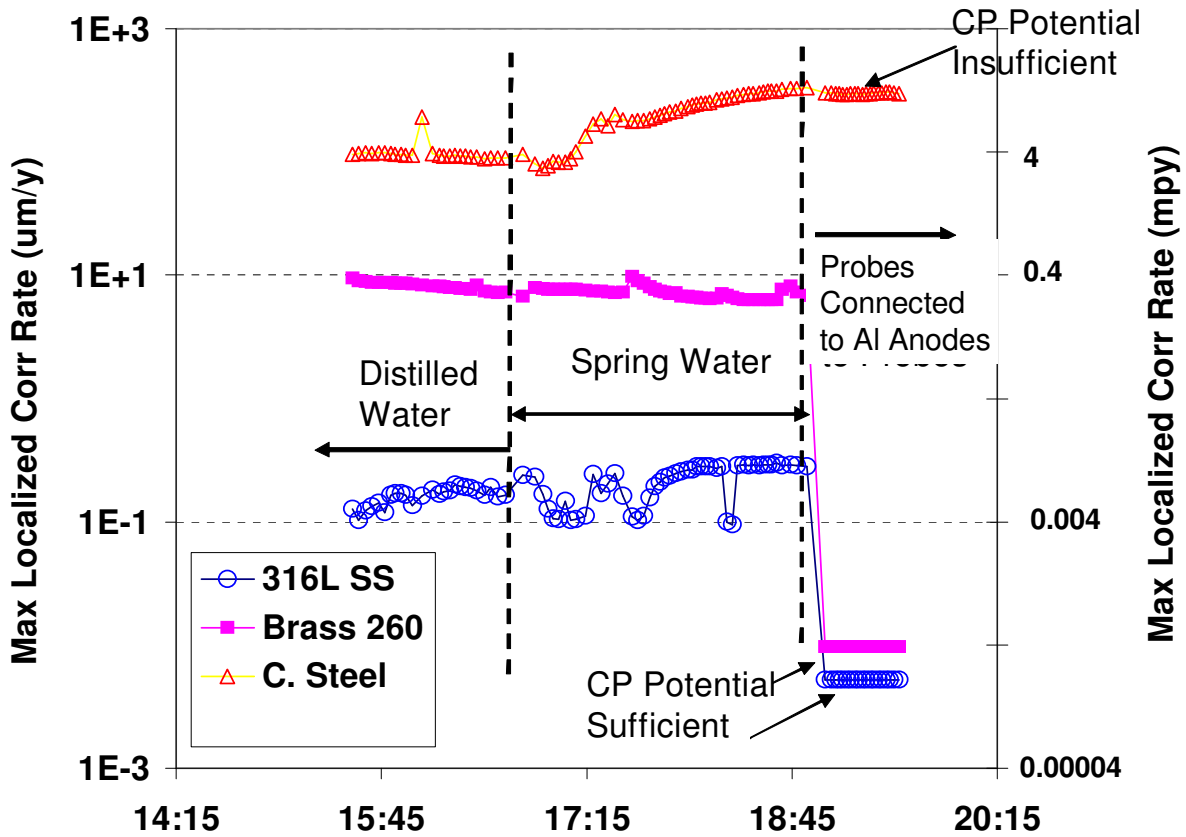
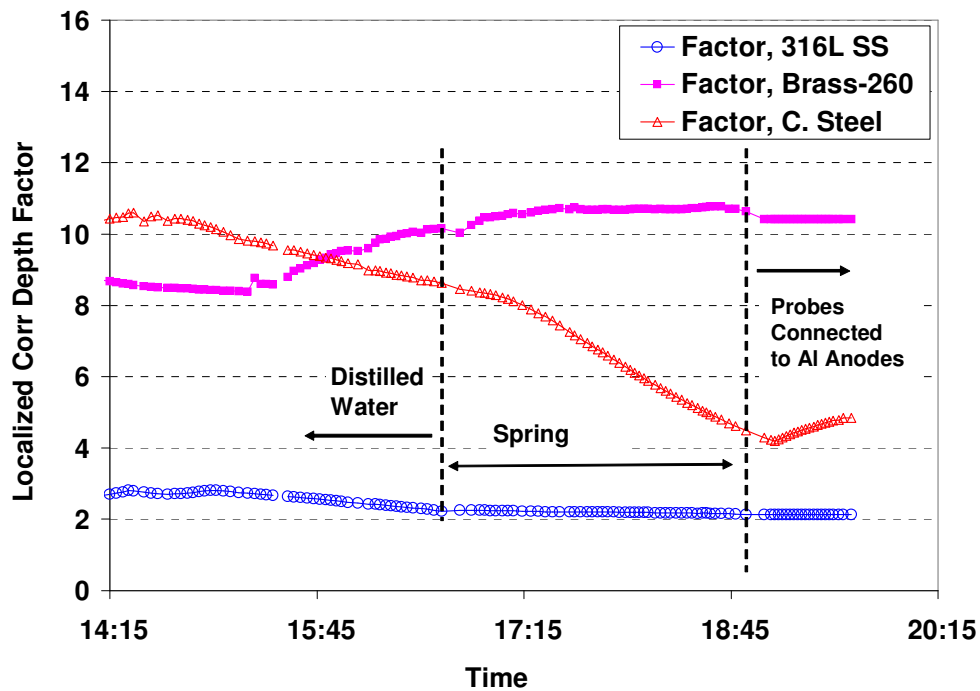**Figure 6 Maximum localized corrosion rates of Type 316L stainless steel, Type 260 brass, and Type 1008 carbon steel probes, during a short-term testing, before and after cathodic protection.**
Note: Probe electrodes were connected to aluminum electrodes to simulate cathodic protection condition (See Figure 4).
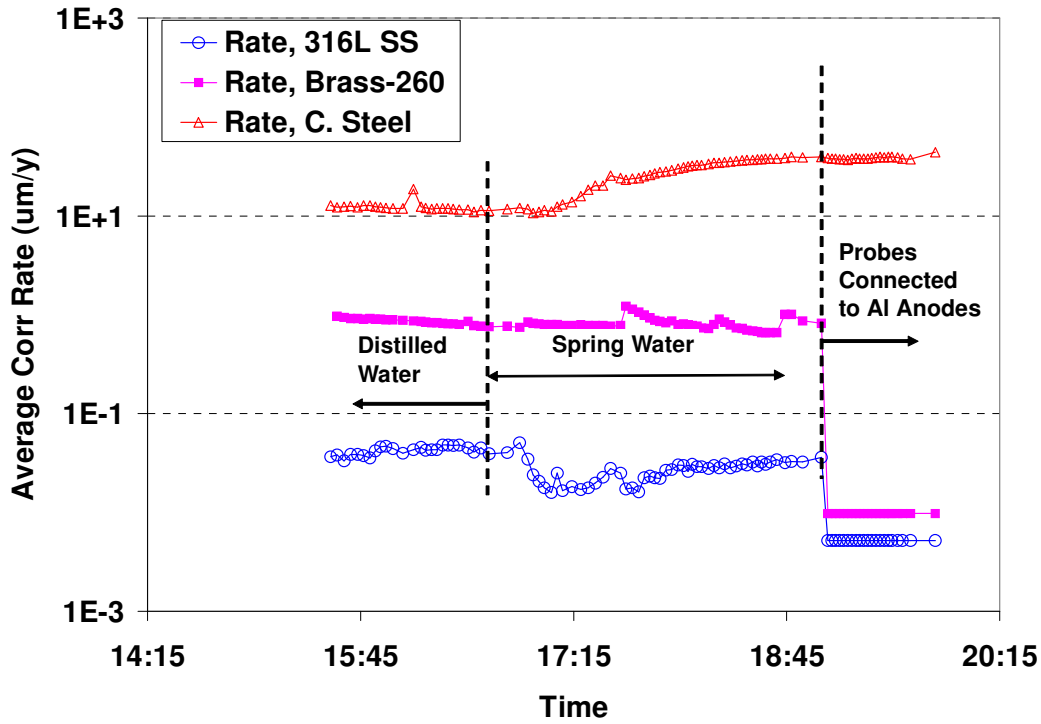
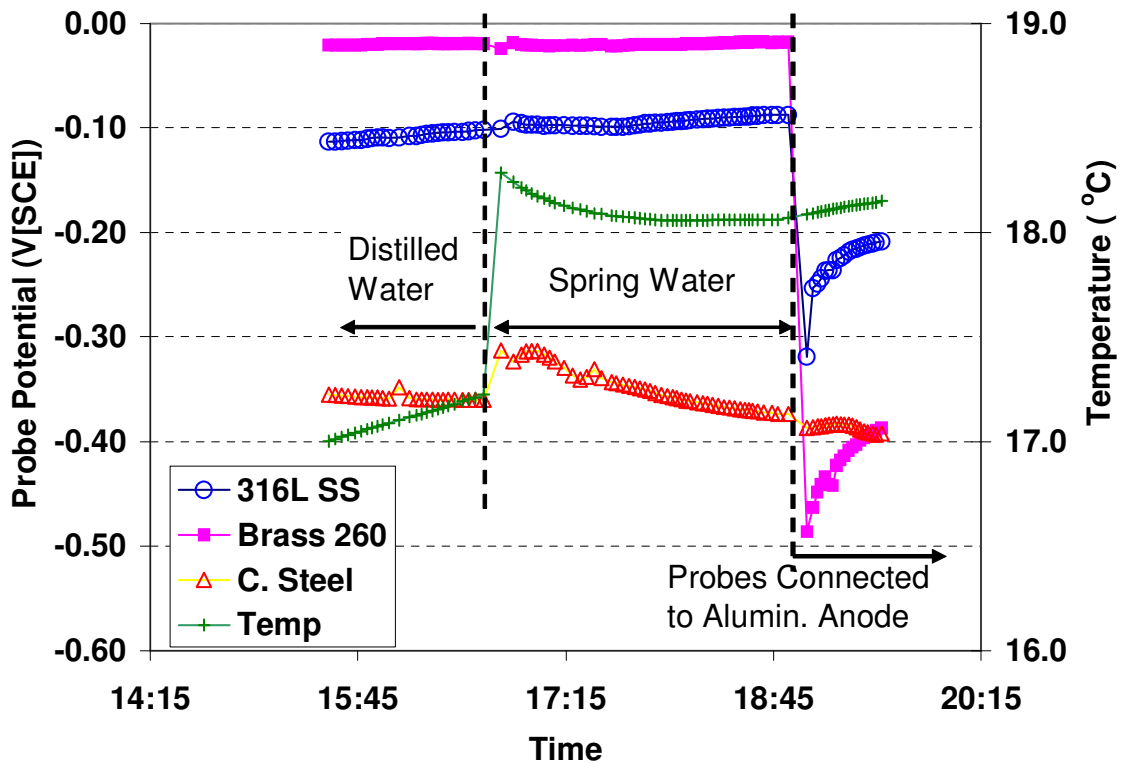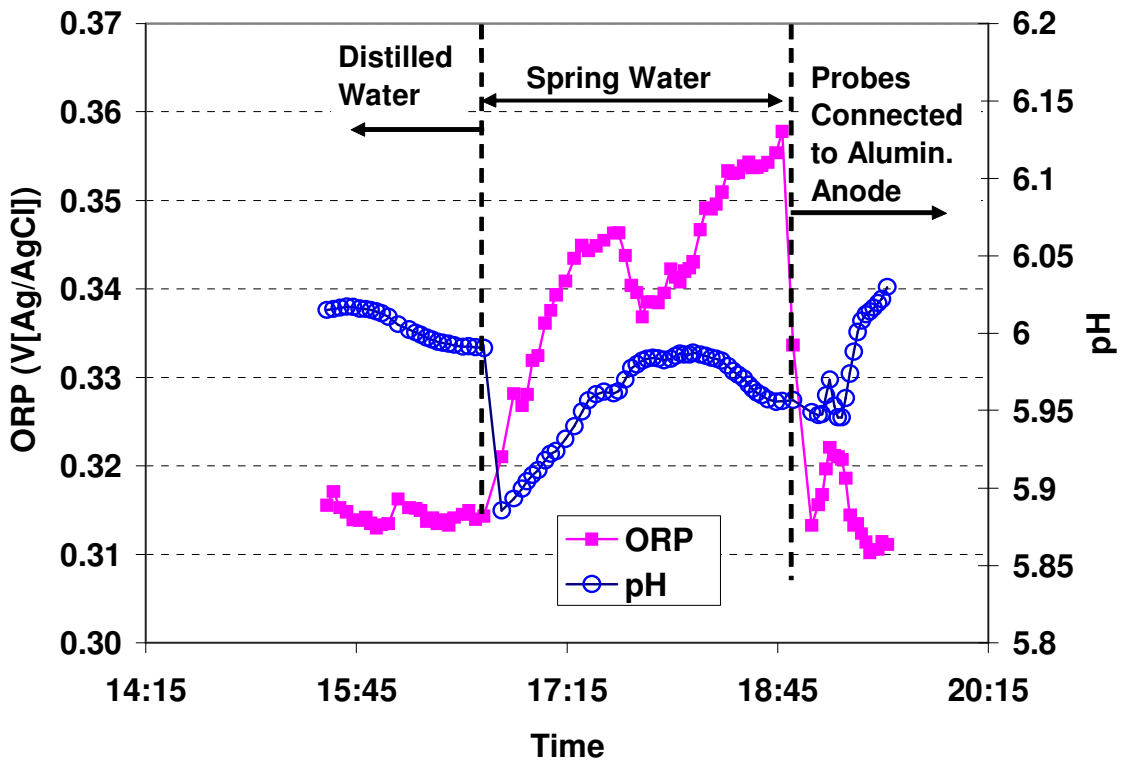**Figure 7 Average corrosion rates of the Type 316L stainless steel, Type 260 brass, and Type 1008 carbon steel probes, during a short-term testing, before and after connecting to aluminum anodes to simulate cathodic protection condition.**
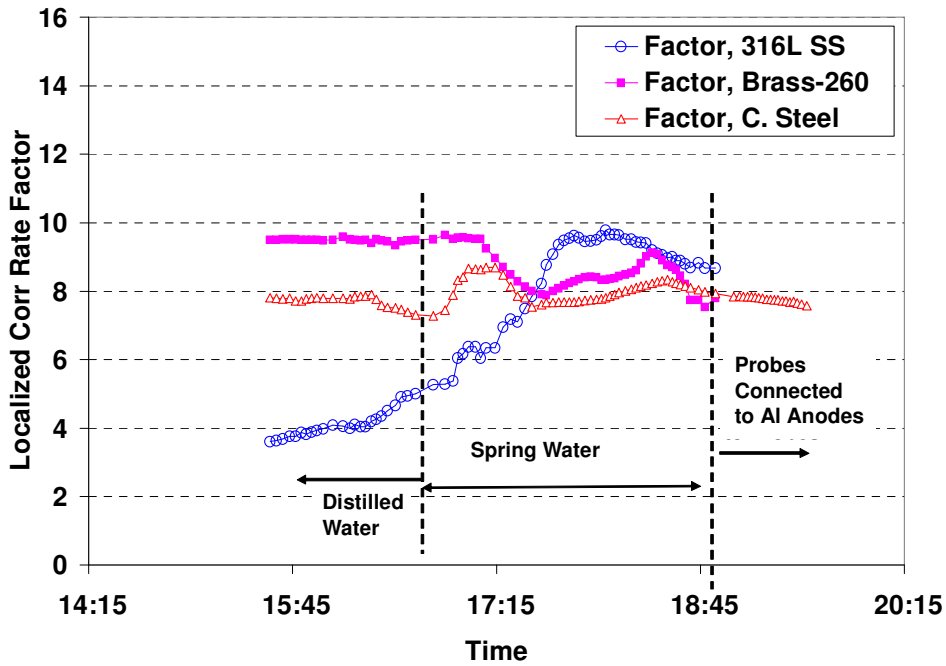
Figure 8. Localized corrosion rate factors of the Type 316L stainless steel, Type 260 brass, and Type 1008 carbon steel probes, during a short-term testing.
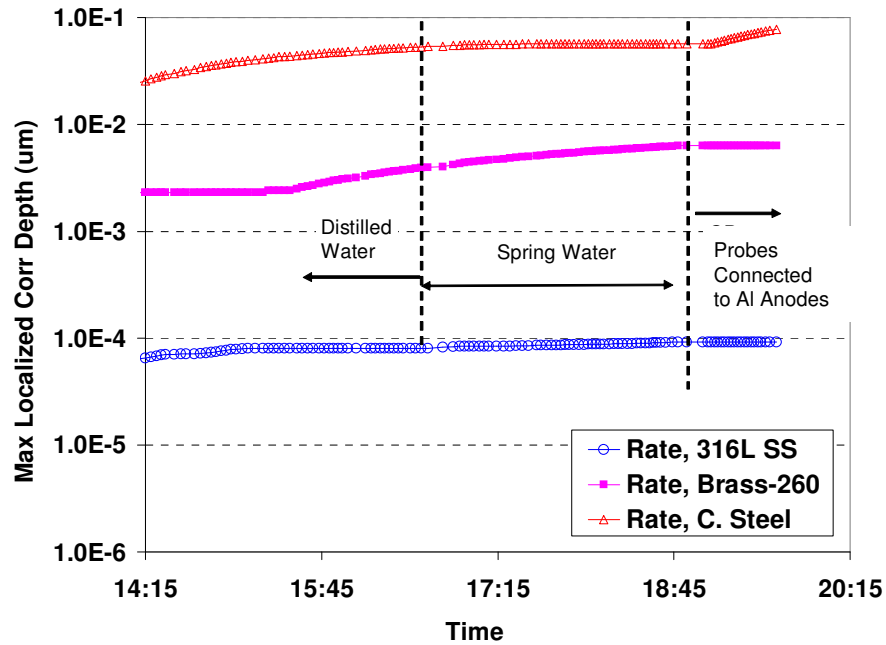
Figure 9. Maximum localized corrosion penetration depths for the Type 316L stainless steel, Type 260 brass, and Type 1008 carbon steel probes, during a short-term testing.
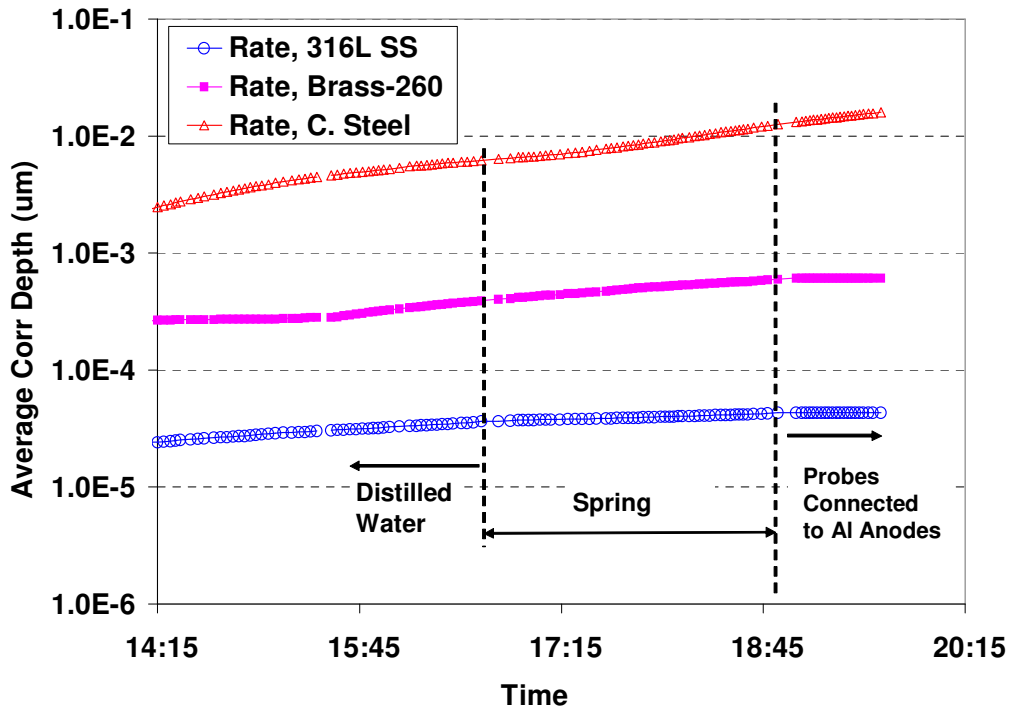
Figure 10. Average corrosion penetration depths for the Type 316L stainless steel, Type 260 brass, and Type 1008 carbon steel probes, during a short-term testing.

Figure 11. Maximum Localized corrosion penetration depth factors for the Type 316L stainless steel, Type 260 brass, and Type 1008 carbon steel probes, during a short-term testing.

Figure 12. Electrochemical potentials of the Type 316L stainless steel, Type 260 brass and Type 1008 carbon steel probes and temperature of the water, during a short-term testing, before and after cathodic protection.

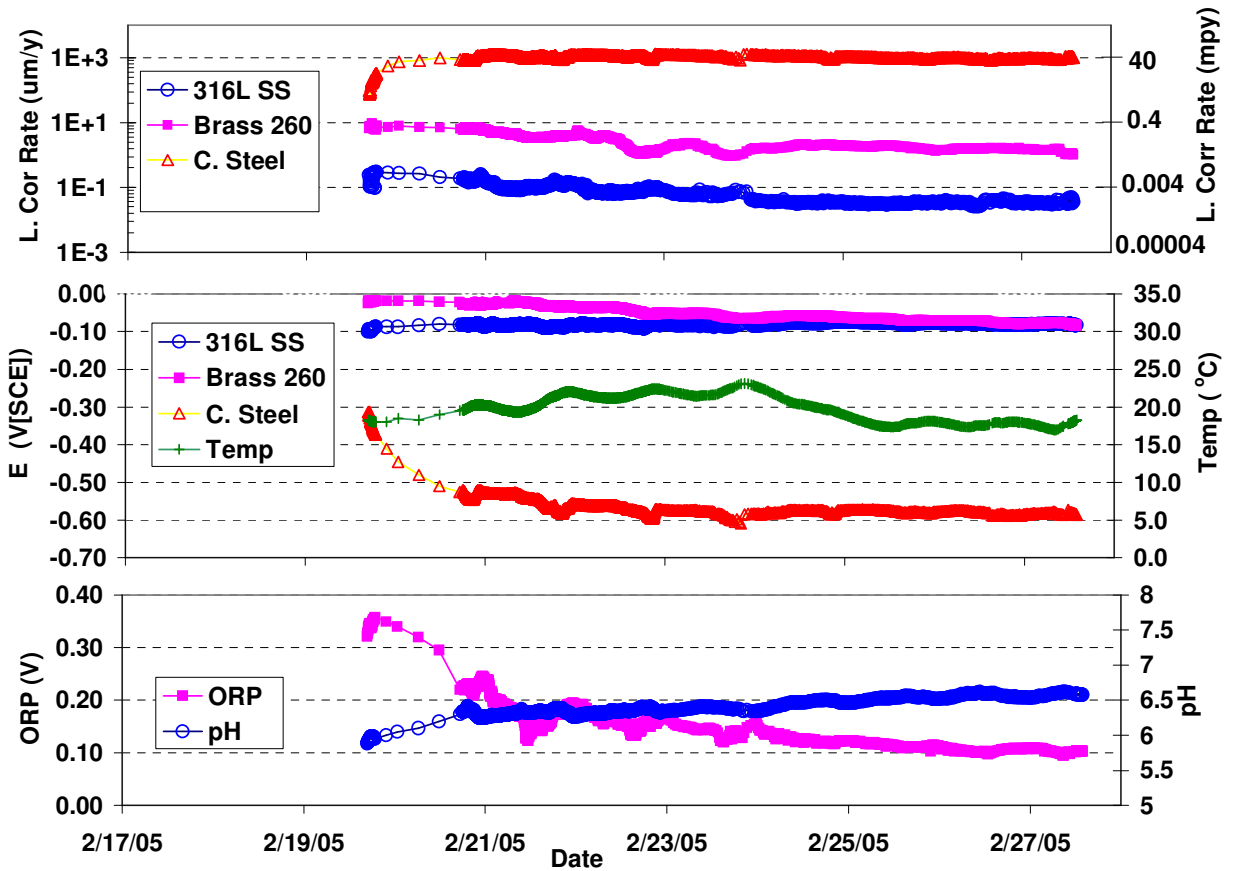**Figure 13. The pH and ORP of the waters during the short-term testing.**

Figure 14. Maximum localized corrosion rates and potentials of the Type 316L stainless steel, Type 260 brass and Type 1008 carbon steel probes and temperature, and the pH and ORP of the water during a longer-term testing in spring water.
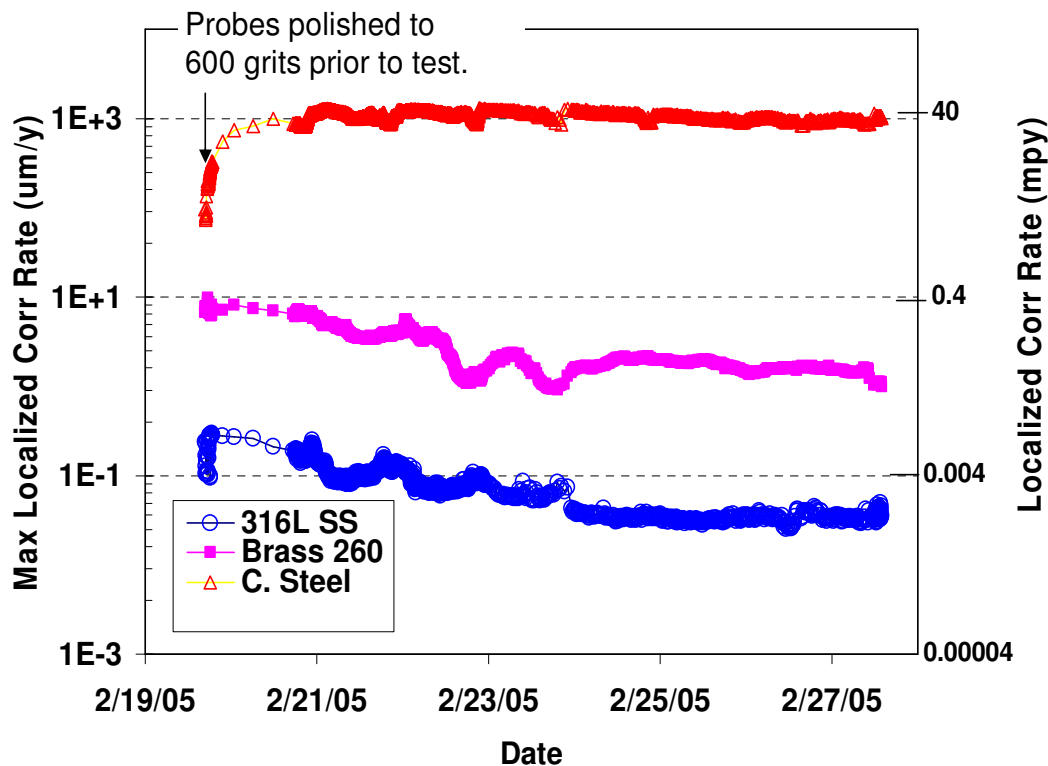
Figure 15. Maximum localized corrosion rates of the Type 316L stainless steel, Type 260 brass and Type 1008 carbon steel probes in spring water.
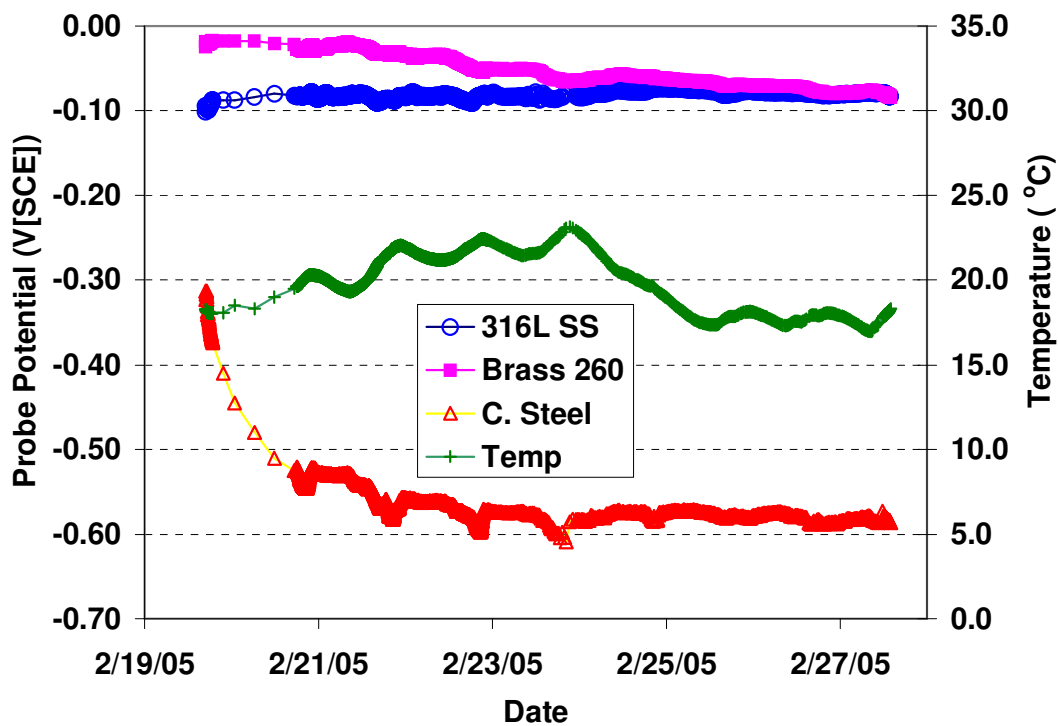

Figure 16. Electrochemical potentials of the Type 316L stainless steel, Type 260 brass and Type 1008 carbon steel probes, and temperature during the test in spring water.
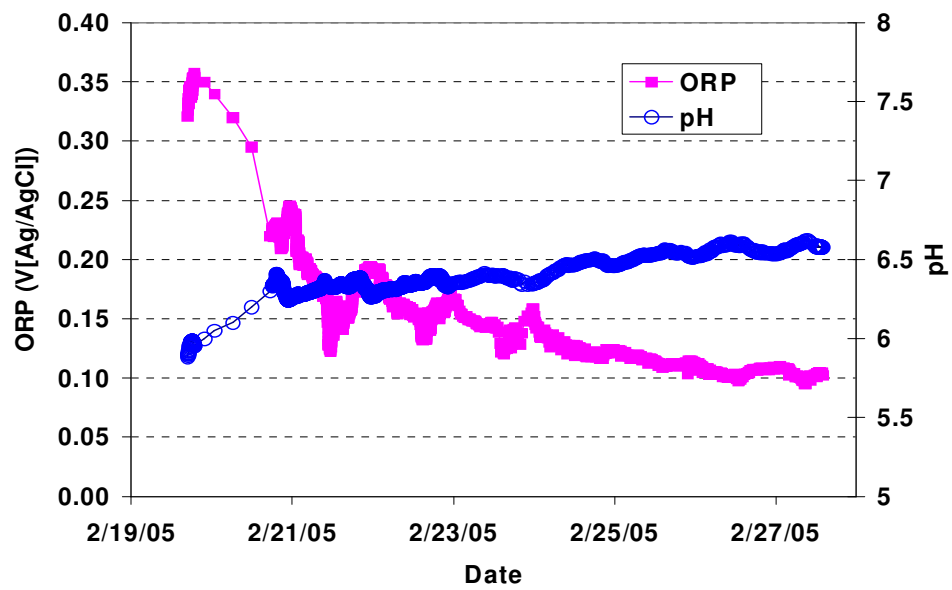
20

Figure 17. The pH and ORP of the spring water during the longer-term testing.
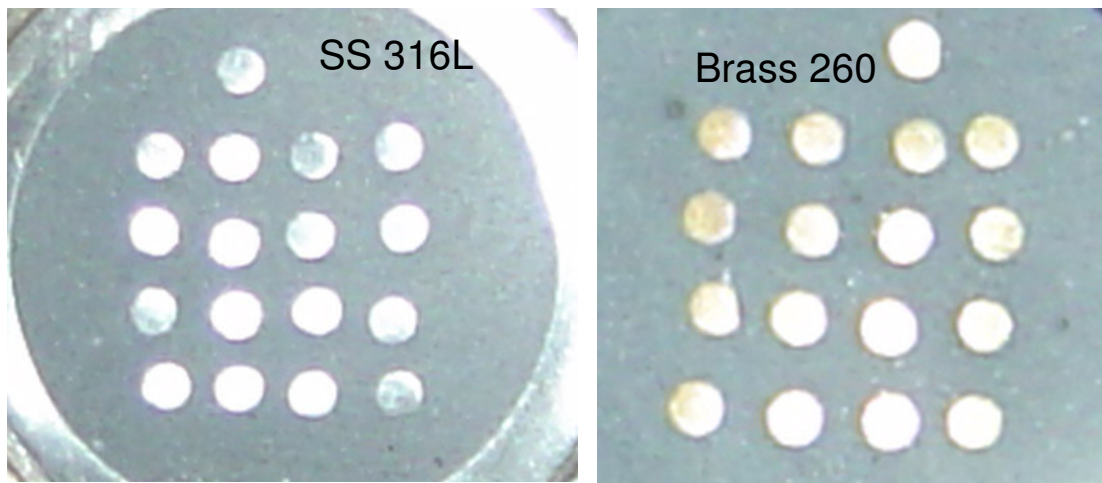
Figure 18. The appearance of the electrodes on the Type 316L stainless steel and Type 269 brass probes prior to cleaning, after the eight-day immersion test in spring water.

Note: Effective electrodes are in the 4 by 4 array. The electrodes shown outside of the 4 by 4 arrays were not coupled to the other electrodes; they served as the position indicator only.
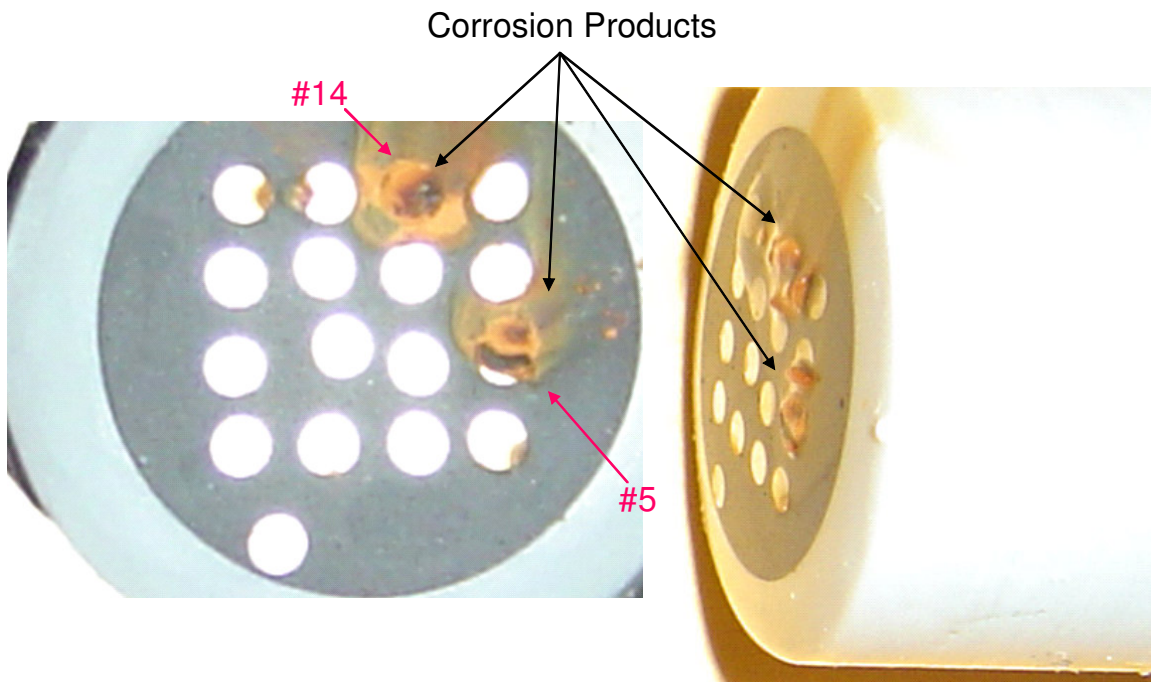

Figure 19. The appearance of the electrodes on the Type 1008 carbon steel probe prior to cleaning, after eight-day immersion in spring water.

Note: The electrode shown outside of the 4 by 4 array was not coupled to the other electrodes; it served as a position indicator only. Electrodes #14 and #5 were mostly covered by corrosion products.